ACS OMEGA

http://pubs.acs.org/journal/acsodf

Article

Au NP-Decorated g-C_3N_4-Based Photoelectochemical Biosensor for Sensitive Mercury Ions Analysis

Mengjie Li,* Ying Wu, Siyu An, and Zhitao Yan

Cite This: *ACS Omega* 2022, 7, 19622−19630

Read Online

ACCESS | Metrics & More | Article Recommendations

ABSTRACT: Herein, an efficient and feasible photoelectrochemical (PEC) biosensor based on gold nanoparticle-decorated graphitic-like carbon nitride (Au NPs@g-C_3N_4) with excellent photoelectric performance was designed for the highly sensitive detection of mercury ions (Hg^{2+}) . The proposed Au NPs@g-C_3N_4 was first modified on the surface of the electrode, which possessed a remarkable photocurrent conversion efficiency and could produce a strong initial photocurrent. Then, the thymine-rich DNA (S1) was immobilized on the surface of the modified electrode via Au−N bonds. Subsequently, 1-hexanethiol (HT) was added to the resultant electrode to block nonspecific binding sites. Finally, the target Hg^{2+} was incubated on the surface of the modified glassy carbon electrode (GCE). In the presence of target Hg^{2+}, the thymine−Hg^{2+}−thymine (T-Hg^{2+}-T) structure formed due to the selective capture capability of thymine base pairs toward Hg^{2+}, resulting in the significantly decrease of the photocurrent. Thereafter, the proposed PEC biosensor was successfully used for sensitive Hg^{2+} detection, as it possessed a wide linear range from 1 pM to 1000 nM with a low detection limit of 0.33 pM. Importantly, this study demonstrates a new method of detecting Hg^{2+} and provides a promising platform for the detection of other heavy metal ions of interest.

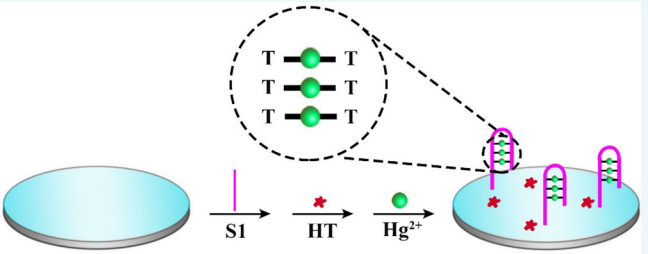

1. INTRODUCTION

In recent years, with the rapid development of industrialization, the accumulation of heavy metal ions in the environment has increased, which has drawn more and more attention to the pollution problem. In terms of environmental pollution, mercury ions (Hg^{2+}) are some of the most toxic heavy metal ions, which are a great threat to human life. An excessive content of Hg^{2+} would cause genetic mutation, affect the cell inheritance, produce teratogenesis, and cause cancer.[1−6] Therefore, the sensitive detection of Hg^{2+} has been an important issue in the fields of environmental and human health. At present, many methods such as colorimetry,[7,8] fluorescence,[9,10] electrochemiluminescence[11−15] and electrochemistry[16,17] have been used to analyze of Hg^{2+}. However, these methods still exhibit the problems of insufficient detection range, poor sensitivity, and expensive equipment. In order to overcome the limitations of the above methods, a novel, sensitive, and accurate Hg^{2+} detection method urgently needs to be established. As a new and developing analytical technology, photoelectrochemical (PEC) biosensors combine optical and electrochemical methods[18−25] and possess the advantages of high sensitivity, excellent selectivity, simple equipment, and low cost. This technology has been widely used in various fields such as biological analysis, the pharmaceutical industry, environmental monitoring, and food safety.[26−32] Given these advantages, the PEC assay might be a promising analytical approach for the development of a highly sensitive and accurate Hg^{2+} detection strategy.

Choosing appropriate photoelectric materials is the key to constructing a highly sensitive PEC sensing platform. Among numerous photoelectric materials, graphitic-like carbon nitride (g-C_3N_4) has a band gap of 2.7 eV, which has attracted wide attention due to g-C_3N_4's excellent chemical stability, adjustable electronic structure, low price, convenient synthesis, and lack of toxicity.[33−38] Unfortunately, the photoelectric performance of g-C_3N_4 is limited by the quick recombination rate of photogenerated electron−hole pairs and its low specific surface area. In order to improve the photoelectric performance of g-C_3N_4, many researchers have focused on modifying g-C_3N_4 to boost the charge separation through element doping, sensitization, and semiconductor coupling.[39,40] In particular, a semiconductor modified with metal nanoparticles (NPs) could effectively improve the photoelectric performance of the semiconductor for two reasons. One is that metal nanoparticles, a type of conductive material with a large specific

Received: March 6, 2022
Accepted: May 6, 2022
Published: May 30, 2022

surface area and unique photoelectric performance, could promote electron capture and transfer in the semiconductor. More importantly, the surface plasmon resonance (SPR) phenomenon would occur with the introduction of metal nanoparticles, which could lead to the enhancement of the light absorption capacity and the charge transfer capacity of semiconductor.[41−45] Inspired by these, we tried to combine g-C_3N_4 with gold nanoparticles (Au NPs) to prepare the Au NPs@g-C_3N_4 complex. In consequence, we have found that as-prepared Au NPs@g-C_3N_4 possessed an excellent photoelectric performance and could be used as an appropriate and promising photoelectric material for the construction of a PEC biosensor.

In this study, Au NPs@g-C_3N_4 as the photoelectric material was employed to construct a PEC biosensor to realize the highly sensitive and selective detection of Hg^{2+}, which is shown in Scheme 1. First, Au NPs@g-C_3N_4 was modified on the

Scheme 1. Schematic Representation of the PEC Biosensor for Hg^{2+} Detection

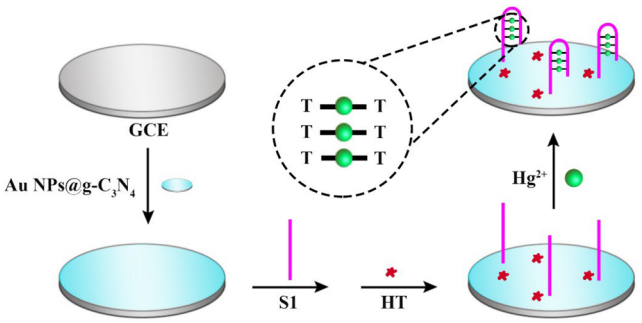

electrode surface to generate a strong initial photocurrent signal. Afterward, the thymine-rich DNA (S1) was immobilized on the modified glassy carbon electrode (GCE) surface via Au−N bonds. Next, 1-hexanethiol (HT) was coated on the electrode surface to block nonspecific adsorption sites. Ultimately, Hg^{2+} was added, and the stable T−Hg^{2+}−T coordination complex formed through the substitution of a proton with the nitrogen atom at thymine position 3 in the DNA molecule. The obtained T−Hg^{2+}−T structure could block electron transfer, leading to an obviously decreased photocurrent signal for the detection of Hg^{2+}. As expected, the PEC biosensor based on Au NPs@g-C_3N_4 exhibited high sensitivity, excellent selectivity, and stability for the Hg^{2+} assay, paving a new pathway for sensitive detection of other heavy metal ions.

2. EXPERIMENTAL SECTION

2.1. Materials and Reagents. Chemical Reagent Co. Ltd. (Chongqing, China) provided H_2O_2. $HAuCl_4{\cdot}4H_2O$ was obtained from China National Medicines Corporation Ltd. (Beijing, China). HT, Tris-HCl buffer, and $K_3[Fe(CN)_6]$ were bought from Shanghai Macklin Biochemical Co., Ltd. (Shanghai, China). KCl, NaCl, $CaCl_2$, $MgCl_2{\cdot}6H_2O$, $Pb(NO_3)_2$, and $Hg(NO_3)_2$ were purchased from Chengdu Kelong Chemical Co., Ltd. (Chengdu, China). This experiment used 0.1 M phosphate buffer solutions (PBS) (pH 7.0), including 0.1 M KCl, 0.1 M Na_2HPO_4 and 0.1 M KH_2PO_4. Ultrapure water was employed to prepare the solutions in this work. The oligonucleotide (S1) was synthesized by Sangon Inc. (Shanghai, China), and its sequence was as follows: 5′-NH_2-CAAATGAACTTTGGTTTCCCTTTTCATTTT-3′.

2.2. Apparatus. The PEC measurement was carried out on a CHI 660E electrochemistry workstation with the help of the TPEC10W LED light source. A three-electrode system, which contained a platinum wire counter electrode, a calomel (saturated KCl) reference electrode, and a glassy carbon working electrode (GCE, Φ = 4 mm), was utilized in this work. A CHI 660E electrochemistry workstation (Shanghai Chenhua Instrumission, China) was also used for electrochemical measurements. The morphology of the nanomaterial was characterized by scanning electron microscopy (SEM, JSM-7800F, Japan) and transmission electron microscopy (TEM, FEI talos F200X, United States). Elemental analysis was performed on an X-ray photoelectron spectrometer (XPS, ESCALAB 250Xi, United States).

2.3. Preparation of g-C_3N_4 and Au NPs@g-C_3N_4. g-C_3N_4 was prepared based on the literature.[46] First, 5 g of melamine was put into a crucible and dried for 24 h at 80 °C, then calcined in a muffle furnace for 3 h. The calcination temperature was 550 °C, and the heating rate was 5 °C·min^{-1}. The obtained product was a powder, and its color was light yellow. Finally, the product was thoroughly washed with 0.1 M nitric acid and ultrapure water.

Au NPs@g-C_3N_4 could be synthesized by an in situ reduction method.[47] Into 5 mL of the 2.0 mg·mL^{-1} g-C_3N_4 solution was dropped 20 μL of 10 mM $HAuCl_4$, and the solution was then stirred in the dark for 2 h. Next, the newly prepared $NaBH_4$ (30 μL, 0.01 M) was added to the above solution drop by drop, and the mixture was stirred continuously. When the gas evolution stopped, the reaction was complete. Subsequently, the obtained solution was placed in a centrifuge and washed by centrifugation to remove impurities. Finally, Au NPs@g-C_3N_4 was stored at 4 °C for subsequent experiments.

2.4. Construction of the PEC Biosensor. The GCE was fully polished with α-Al_2O_3 powder and then washed with ultrapure water before modification. Then, the clean GCE was coated with 10 μL of the as-prepared Au NPs@g-C_3N_4 solution and dried at 37 °C To generate a uniform film. Subsequently, the Au NPs@g-C_3N_4-modified electrode was incubated with 5 μL of 2 μM thymine-rich DNA (S1) at 4 °C overnight. S1 could be stably immobilized on the surface of Au NPs@g-C_3N_4/GCE via a Au−N bond. After the sample was blocked with 10 μL of 1 mM HT for 40 min, 10 μL of Hg^{2+} solutions with different concentrations was dropped onto the modified electrode. The sample was incubated at 37 °C for 1 h. In the presence of Hg^{2+}, the T-rich DNA (S1) could recognize and capture Hg^{2+} and quickly folded into the T−Hg^{2+}−T structure, thus quenching the photocurrent signal. The construction process of the PEC biosensor was shown in Scheme 1.

2.5. PEC Measurement. The PEC measurement was performed in 5 mL of 0.1 M PBS containing 40 μL H_2O_2, where H_2O_2 was the electron donor. The LED lamp with a wavelength of 365−370 nm served as the excitation light source and was switched off, on, and off for 10, 20, and 10 s, respectively, under a 0.0 V potential.

3. RESULTS AND DISCUSSION

3.1. Characterization of the Different Materials. The morphology of the prepared material was characterized by SEM. As displayed in Figure 1A, the SEM image showed that

https://doi.org/10.1021/acsomega.2c01335
ACS Omega 2022, 7, 19622−19630

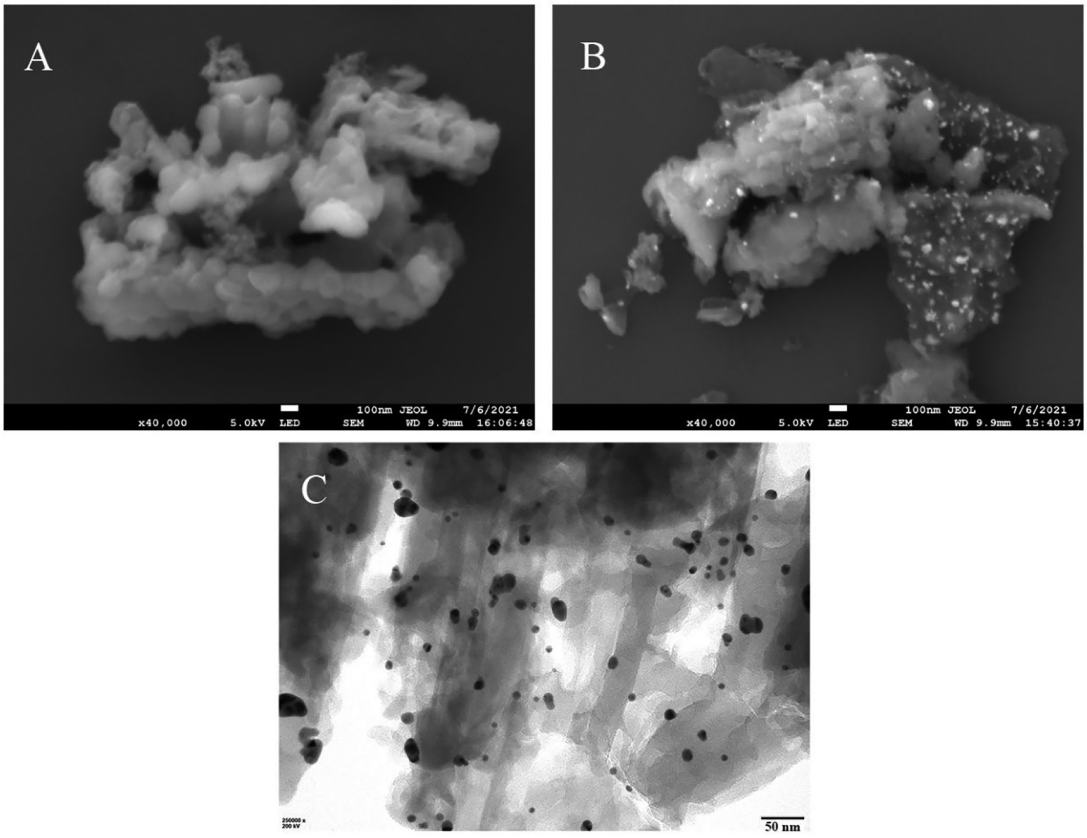

Figure 1. SEM images of (A) g-C_3N_4 and (B) Au NPs@g-C_3N_4. (C) TEM image of Au NPs@g-C_3N_4.

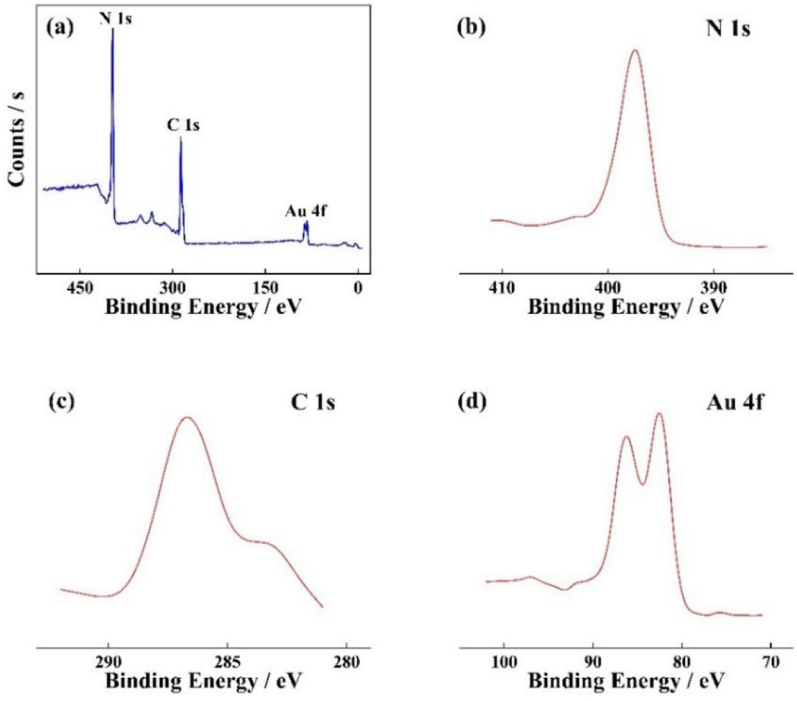

Figure 2. XPS analysis of (a) the full region of Au NPs@g-C_3N_4, (b) the N 1s region, (c) the C 1s region, and (d) the Au 4f region.

the sample of g-C_3N_4 presented a layered structure with a mist-like edge. The diameter of g-C_3N_4 was about 110 nm. The SEM image of Au NPs@g-C_3N_4 is displayed in Figure 1B. It was observed that the surface of g-C_3N_4 was coated with numerous Au NPs. Meanwhile, TEM was also used to morphologically characterize Au NPs@g-C_3N_4. As shown in Figure 1C, a large number of small black spots of Au NPs were evenly distributed on the surface of g-C_3N_4. After being linked

https://doi.org/10.1021/acsomega.2c01335
ACS Omega 2022, 7, 19622−19630

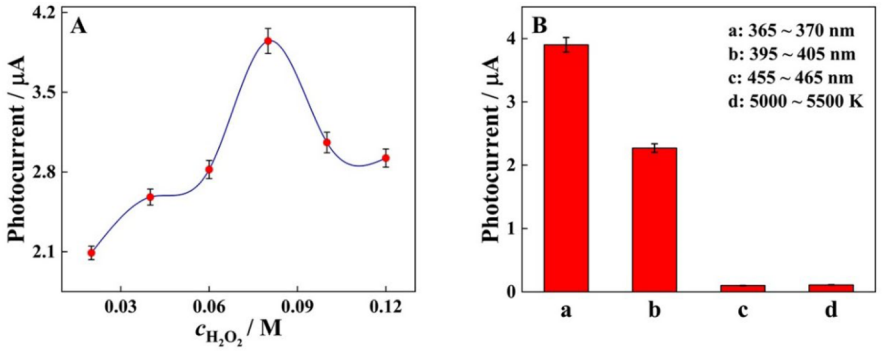

Figure 3. Effect of (A) the H_2O_2 concentration in the detection solution and (B) the irradiation wavelength on the photocurrent.

with Au NPs, the average size increased by about 10 nm. Additionally, these results were in accordance with the literature,[48−50] which showed that g-C_3N_4 and Au NPs@g-C_3N_4 were successfully synthesized.

In addition, XPS was used for elemental analysis. As shown in Figure 2, the peaks at 397 and 286 eV might correspond to N 1s and C 1s, respectively. This was consistent with literature, indicating the presence of N and C elements.[51−53] Moreover, the peaks at 82 and 86 eV confirmed the presence of the Au element.[54,55] These results demonstrated the successful preparation of Au NPs@g-C_3N_4.

3.2. Condition Optimization. To obtain an excellent analytical performance, the concentration of H_2O_2 in 5 mL of PBS and the wavelength of emitted light were optimized. As illustrated in Figure 3A, when the concentration of H_2O_2 increased from 0.02 to 0.08 M, the photocurrent also increased. However, the photocurrent decreased when the concentration of H_2O_2 increased from 0.08 to 0.12 M. Therefore, the optimal concentration of H_2O_2 was 0.08 M, corresponding to the photocurrent of 3.9 μA. As shown in Figure 3B, no significant photocurrent was observed at irradiation wavelengths of 455−465 nm and the mixed white light of 5000−5500 K. A photocurrent of about 2.27 μA could be found at 395−405 nm. However, when the irradiation wavelength was 365−370 nm, the photocurrent was the highest at 3.9 μA. Therefore, the optimal irradiation wavelength in this work was 365−370 nm.

3.3. Comparison of PEC Signals of Different Materials. In order to prove the superiority of Au NPs@g-C_3N_4 as a photoelectric material, PEC signals of g-C_3N_4 and Au NPs@g-C_3N_4 were compared under the same experimental conditions. As illustrated in Figure 4, the PEC signal of g-C_3N_4 was 1.3 μA. Au NPs@g-C_3N_4 produced a higher PEC signal, which was almost three times larger than that of g-C_3N_4, because the existence of Au NPs could produce a strong SPR enhancement effect. From the result, it could be seen that Au NPs@g-C_3N_4 performed better than g-C_3N_4.

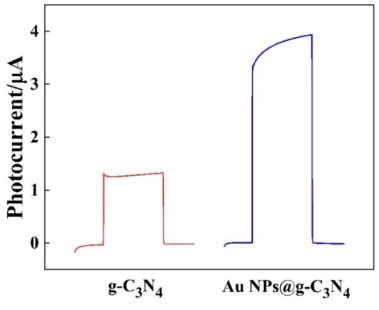

Figure 4. PEC signals of g-C_3N_4 and Au NPs@g-C_3N_4.

3.4. PEC Mechanism of the Biosensor. Figure 5A shows the electron transfer process after the incubation of Au NPs@g-C_3N_4 on the GCE surface. g-C_3N_4 absorbed the light energy, and the electrons were excited into its conduction band (CB). One part of the photogenerated electrons was transferred to the electrode, and the other part was transferred to Au NPs. At the same time, Au NPs would be excited by incident light, causing electrons to oscillate collectively due to the SPR effect. After that, these electrons could immediately move to electrode. In addition, H_2O_2 as an electron donor contributed electrons to the valence band (VB) of g-C_3N_4. A strong photocurrent signal would be generated, as seen in Figure 5A. Figure 5B is the electron transfer diagram of photocurrent quenching after the addition of Hg^{2+}. The T−Hg^{2+}−T structure formed by thymine-rich DNA (S1) and Hg^{2+} would produce the steric hindrance effect, which could reduce the ability of light to capture electrons and prevent H_2O_2 from providing electrons. In addition, the photogenerated electrons produced from g-C_3N_4 and Au NPs could flow to the T−Hg^{2+}−T structure because Hg^{2+} possessed the electron-withdrawing property. As a result, the photocurrent signal was greatly quenched.

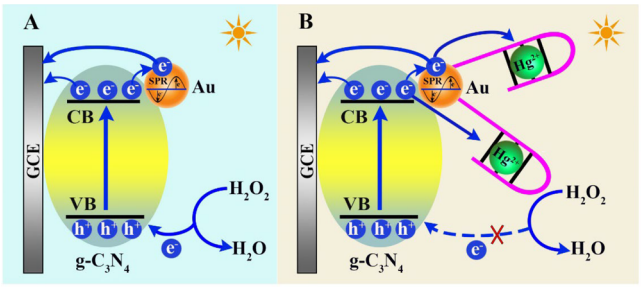

Figure 5. Mechanisms for (A) photocurrent generation and (B) photocurrent quenching.

3.5. PEC Characterization of the Biosensor. In order to confirm the successful construction of the PEC biosensor, photocurrent characterization was carried out step by step. As seen in Figure 6, after Au NPs@g-C_3N_4 were incubated on the bare GCE surface, a sharply enhanced photocurrent was observed (curve b) compared with that of the bare GCE (curve a), mainly due to the favorable photoelectric properties of Au NPs@g-C_3N_4. The photocurrent evidently decreased (curve c) with the immobilization of S1 due to the poor

https://doi.org/10.1021/acsomega.2c01335
ACS Omega 2022, 7, 19622−19630

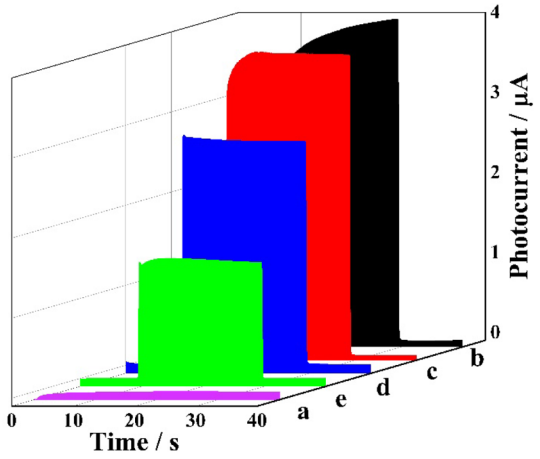

Figure 6. Photocurrent of (a) bare GCE, (b) Au NPs@g-C_3N_4/GCE, (c) S1/Au NPs@g-C_3N_4/GCE, (d) HT/S1/Au NPs@g-C_3N_4/GCE, and (e) Hg^{2+}/HT/S1/Au NPs@g-C_3N_4/GCE.

conductivity of S1. Afterward, the photocurrent decreased again with addition of HT (curve d). Finally, when Hg^{2+} was modified on the above GCE surface, the photocurrent decreased significantly (curve e) due to the formation of the T−Hg^{2+}−T structure. These results confirmed that the PEC biosensor was constructed successfully.

3.6. Electrochemical Characterization of the PEC Biosensor. In order to study the preparation process of the PEC biosensor, cyclic voltammetry (CV) was used to characterize the peak current of the PEC biosensor at each step. The corresponding electrode was placed in 2 mL of PBS (pH 7, 0.1 M) containing 5.0 mM $[Fe(CN)_6]^{3-/4-}$ and 0.1 M KCl at a scanning rate of 50 mV·s^{-1}. As shown in Figure 7A, the bare electrode (curve a) showed a couple of reversible redox peaks. However, the peak current (curve b) evidently decreased after the modification with Au NPs@g-C_3N_4, which was mainly attributed to the semiconductor properties of Au NPs@g-C_3N_4. With the addition of S1, the peak current (curve c) further decreased because S1 and $[Fe(CN)_6]^{3-/4-}$ both had negative charges and like charges repel each other. When HT was modified on the surface of the electrode, the peak current (curve d) continued to decrease. Finally, after Hg^{2+} was incubated on the electrode's surface, the peak current (curve e) decreased, which was again caused by the formation of T−Hg^{2+}−T structures.

Meanwhile, the processes of the PEC biosensor were also characterized by electrochemical impedance spectroscopy (EIS), which was carried out in 2 mL of PBS (pH 7.0, 0.1 M) with 5.0 mM $[Fe(CN)_6]^{3-/4-}$ and 0.1 M KCl. The frequency range was from 10 kHz to 0.1 Hz, the alternating current potential was 5 mV, and the direct current potential was 0.22 V. As displayed in Figure 7B, compared with bare GCE (curve a), the Au NPs@g-C_3N_4 -incubated electrode exhibited a greater charge-transfer resistance (R_{et}) (curve b) because Au NPs@g-C_3N_4 could hinder electron transfer. After S1 was modified on the surface of Au NPs@g-C_3N_4/GCE, the R_{et} increased once more (curve c) due to the repulsion between negatively charged S1 and $[Fe(CN)_6]^{3-/4-}$. When nonconductive HT was added to the electrode, R_{et} further increased(curve d). R_{et} continued to increase after the sample was incubated with Hg^{2+} (curve e) because of the formation of T−Hg^{2+}−T structures. These results demonstrated that the PEC biosensor was prepared successfully.

3.7. PEC Analysis of Hg^{2+} at the Developed Biosensor. On the basis of the optimal conditions, photocurrents of samples incubated with different concentrations Hg^{2+} were measured to evaluate the analytical performance of the PEC biosensor, as shown in Figure 8A. As the concentration of Hg^{2+} increased from 1 pM to 1000 nM, the photocurrent decreased sharply. Figure 8B shows the linear response curve between the photocurrent and the logarithm of Hg^{2+} concentrations. The regression equation was $I = -0.209\lg c + 2.07$, with a correlation coefficient of 0.998 (where I is the photocurrent and c is Hg^{2+} concentration). The insert of Figure 8B shows the linear response curve between the photocurrent and the Hg^{2+} concentration at a low concentration range. The regression equation was $I = -23.485c + 2.727$. The detection limit (LOD) of 0.33 pM was calculated according to LOD = $3S_B/m$, where S_B was standard deviation of the blank signals and m was the analytical sensitivity. Meanwhile, a comparison was made between the analytical performance of the proposed PEC biosensor and other reported methods, which is illustrated in Table 1. The PEC biosensor constructed in this work had a better sensitivity and a wider linear range, which indicated that this sensing strategy was an excellent potential method for Hg^{2+} detection.

3.8. Selectivity and Stability of the PEC Biosensor. In order to explore the selectivity of the proposed PEC biosensor, several interfering substances were evaluated, including Pb^{2+}, Na^+, Ca^{2+}, Mg^{2+}, and K^+. As shown in Figure 9A, after the sample was incubated with 100 nM interfering substances, the obvious photocurrents were obtained. The photocurrent of the

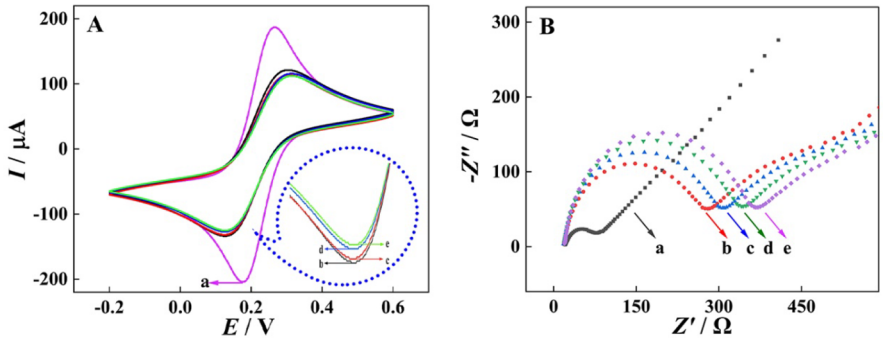

Figure 7. (A) CV and (B) EIS responses of (a) bare GCE, (b) Au NPs@g-C_3N_4/GCE, (c) S1/Au NPs@g-C_3N_4/GCE, (d) HT/S1/Au NPs@g-C_3N_4/GCE, and (e) Hg^{2+}/HT/S1/Au NPs@g-C_3N_4/GCE.

https://doi.org/10.1021/acsomega.2c01335
ACS Omega 2022, 7, 19622−19630

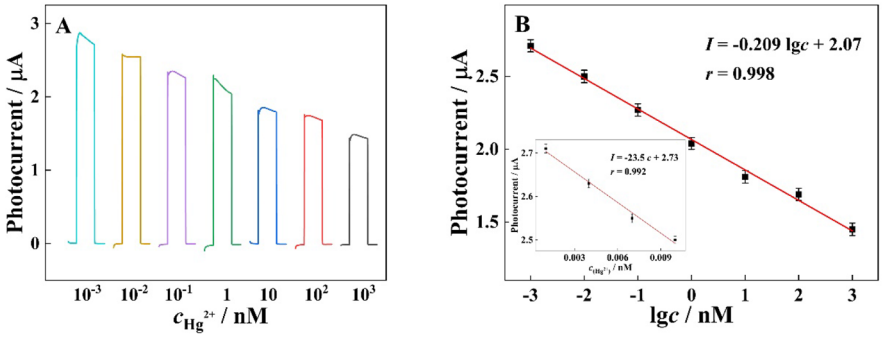

Figure 8. (A) Photocurrent with various Hg^{2+} concentrations. (B) Linear relationship between the photocurrent and the logarithm of the Hg^{2+} concentration. The insert in panel B presents the calibration curve of the photocurrent value vs the concentration of Hg^{2+} at a low concentration range.

Table 1. Comparison of Different Methods for Hg^{2+} Detection

analytical method	detection limit	linear range	ref.
fluorescence	0.24 nM	10−600 nM	56
fluorescence	15.2 nM	0−350 nM	57
SERS[a]	0.1 nM	0.1−1000 nM	58
colorimetry	20 nM	50−1 mM	59
colorimetry	10.3 nM	0−20 μM	60
electrochemistry	0.13 nM	0.01−0.5 nM	61
PEC	5.7 pM	10 pM to 1.0 μM	62
PEC	0.33 pM	1 pM to 1000 nM	our work

[a]Surface-enhanced Raman scattering spectra.

interfering substance was almost the same as that of the blank sample. However, when 1 nM Hg^{2+} was incubated, the photocurrent significantly decreased. The result showed that the PEC biosensor had an excellent selectivity for Hg^{2+} detection because the T−T mismatch bases had a high affinity for Hg^{2+}. In addition, the stability of this PEC biosensor was investigated by recording the photocurrent of 1 nM Hg^{2+}-incubated PEC biosensor under nine consecutive cycles of "off−on−off" light. It can be seen in Figure 9B that the photocurrent was stable with a relative standard deviation (RSD) of 0.417%, which indicated that the proposed PEC biosensor possessed a good stability for Hg^{2+} detection.

3.9. Preliminary Application of Hg^{2+} Detection. The standard addition method was applied to evaluate the applicability and reliability of the constructed PEC biosensor. Different concentrations of Hg^{2+} were added into water and detected using this biosensor. As can be seen in Table 2, the concentrations of Hg^{2+} were 500 nM, 50 nM, 500 pM, 50 pM, and 5 pM, and the corresponding recovery rates were 95.6%, 105.6%, 94.6%, 94.6%, and 103.2%. The above results indicated that the proposed PEC biosensor had great potential to detect Hg^{2+} in real samples.

Table 2. Detection of Hg^{2+} with different concentrations by PEC biosensor

sample number	added (nM)	found (nM)	recovery (%)
1	500	478	95.6
2	50.0	52.8	105.6
3	5.00×10^{-1}	4.73×10^{-1}	94.6
4	5.00×10^{-2}	4.73×10^{-2}	94.6
5	5.00×10^{-3}	5.16×10^{-3}	103.2

4. CONCLUSIONS

In summary, a novel and sensitive PEC biosensor has been developed for Hg^{2+} detection based on Au NPs@g-C_3N_4 as the photoelectric material. The prepared Au NPs@g-C_3N_4 could provide an excellent initial photocurrent signal because the introduction of Au NPs to the surface of g-C_3N_4 could lead to the SPR phenomenon, thus enhancing both the absorption of visible light and the electron transfer ability. Besides, the chemical coordination of T−Hg^{2+}−T between S1 and Hg^{2+} could hinder electron transfer, leading to a significant reduction of the PEC signal for achieving the quantitative analysis of Hg^{2+}. The as-proposed PEC biosensor displayed the advantages of simple preparation, sensitive detection, good stability, and high selectivity. Furthermore, this developed PEC strategy provides a modular platform for the analysis of various trace heavy metal ions, which is expected to be applied in environmental and disease detection.

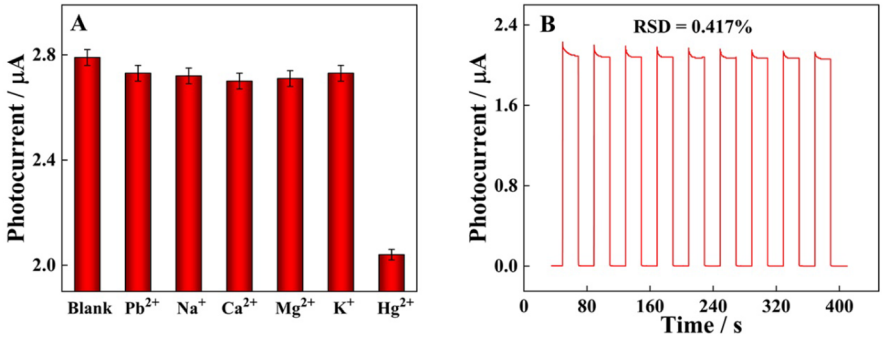

Figure 9. (A) Exploration of the selectivity of the PEC biosensor. (B) Stability test of the biosensor at 1 nM Hg^{2+}.

https://doi.org/10.1021/acsomega.2c01335
ACS Omega 2022, 7, 19622−19630

AUTHOR INFORMATION

Corresponding Author

Mengjie Li − *School of Civil Engineering and Architecture, Chongqing University of Science and Technology, Chongqing 401331, China; Institute for Health and Environment, Chongqing University of Science and Technology, Chongqing 401331, PR China;* orcid.org/0000-0001-8573-7025; Email: mengjieli@cqust.edu.cn

Authors

Ying Wu − *School of Civil Engineering and Architecture, Chongqing University of Science and Technology, Chongqing 401331, China; Institute for Health and Environment, Chongqing University of Science and Technology, Chongqing 401331, PR China*

Siyu An − *School of Civil Engineering and Architecture, Chongqing University of Science and Technology, Chongqing 401331, China; Institute for Health and Environment, Chongqing University of Science and Technology, Chongqing 401331, PR China*

Zhitao Yan − *School of Civil Engineering and Architecture, Chongqing University of Science and Technology, Chongqing 401331, China; Institute for Health and Environment, Chongqing University of Science and Technology, Chongqing 401331, PR China*

Complete contact information is available at: https://pubs.acs.org/10.1021/acsomega.2c01335

Notes

The authors declare no competing financial interest.

ACKNOWLEDGMENTS

This work was financially supported by the Science and Technology Research Program of Chongqing Municipal Education Commission (KJQN202101522) and the Research Start-up Fund for New Faculty of Chongqing University of Science and Technology (ckrc2020024).

REFERENCES

(1) Zhang, L.-X.; Li, P.; Feng, L.-P.; Chen, X.; Jiang, J.-T.; Zhang, S.; Zhang, C.-X.; Zhang, A.-C.; Chen, G.-F.; Wang, H. Synergetic Ag_2S and ZnS quantum dots as the sensitizer and recognition probe: A visible light-driven photoelectrochemical sensor for the "signal-on" analysis of mercury (II). *J. Hazard. Mater.* **2020**, *387*, 121715.

(2) Wu, S.; Zhao, Y.; Deng, X.-X.; Yang, X.-L.; Wang, X.-Y.; Zhao, Y.-Q. Oxygen defects engineered $CdS/Bi_2O_{2.33}$ direct Z-Scheme heterojunction for highly sensitive photoelectrochemical assay of Hg^{2+}. *Talanta* **2020**, *217*, 121090.

(3) Li, Z.-Z.; Zhou, X.; Yang, J.; Fu, B.-H.; Zhang, Z.-H. Near-Infrared-Responsive Photoelectrochemical Aptasensing Platform Based on Plasmonic Nanoparticle-Decorated Two-Dimensional Photonic Crystals. *ACS Appl. Mater. Interfaces* **2019**, *11*, 21417−21423.

(4) Jiang, Q.-Q.; Wang, H.-J.; Wei, X.-Q.; Wu, Y.; Gu, W.-L.; Hu, L.-Y.; Zhu, C.-Z. Efficient $BiVO_4$ photoanode decorated with $Ti_3C_2T_X$ MXene for enhanced photoelectrochemical sensing of Hg(II) ion. *Anal. Chim. Acta* **2020**, *1119*, 11−17.

(5) Hao, Y.-Q.; Cui, Y.-L.; Qu, P.; Sun, W.-Z.; Liu, S.-P.; Zhang, Y.-T.; Li, D.-L.; Zhang, F.-Q.; Xu, M.-T A novel strategy for the construction of photoelectrochemical sensing platform based on multifunctional photosensitizer. *Electrochim. Acta* **2018**, *259*, 179−187.

(6) Zhang, X.-Y.; Li, M.-Y.; He, L.-M.; Tian, D.-D.; Zhang, L.-J.; Zhang, J.-H.; Liu, M. Highly sensitive and selective photoelectrochemical sensor for mercury(II) detection based on efficient Bi_2MoO_6 photoanode decorated with CuS. *J. Alloy. Compd.* **2021**, *864*, 157905.

(7) Yin, M.-Y.; Wan, Y.-Q.; Li, S.; Zhao, X.-T.; Zhang, W.-W.; Zhang, Y.; Wang, H. Carbon nitride-doped melamine-silver adsorbents with peroxidase-like catalysis and visible-light photocatalysis: Colorimetric detection and detoxification removal of total mercury. *J. Hazard. Mater.* **2021**, *408*, 124978.

(8) Wang, J.-H.; Wu, J.-M.; Zhang, Y.-P.; Zhou, X.; Hu, Z.-W.; Liao, X.-J.; Sheng, B.-B.; Yuan, K.-S.; Wu, X.-Q.; Cai, H.-H.; Zhou, H.-B.; Sun, P.-H. Colorimetric and SERS dual-mode sensing of mercury (II) based on controllable etching of Au@Ag core/shell nanoparticles. *Sensors Actuators B Chem.* **2021**, *330*, 129364.

(9) Zhou, X.-Y.; Wang, C.-C.; Wu, L.-N.; Wei, W.; Liu, S.-Q. An OliGreen-responsive fluorescence sensor for sensitive detection of organophosphorus pesticide based on its specific selectivity towards T-Hg^{2+}-T DNA structure. *Spectrochim. Acta, Part A* **2021**, *247*, 119155.

(10) Shi, Y.-Q.; Li, W.-T.; Feng, X.-P.; Lin, L.; Nie, P.-C.; Shi, J.-Y.; Zou, X.-B.; He, Y. Sensing of mercury ions in Porphyra by Copper @ Gold nanoclusters based ratiometric fluorescent aptasensor. *Food Chem.* **2021**, *344*, 128694.

(11) Cao, S.-P.; Luo, Q.-X.; Li, Y.-J.; Liang, R.-P.; Qiu, J. Gold nanoparticles decorated carbon nitride nanosheets as a coreactant regulate the conversion of the dual-potential electrochemiluminescence of $Ru(bpy)_3^{2+}$ for Hg^{2+} detection. *Chem. Commun.* **2020**, *56*, 5625−5628.

(12) Babamiri, B.; Salimi, A.; Hallaj, R. Switchable electrochemiluminescence aptasensor coupled with resonance energy transfer for selective attomolar detection of Hg^{2+} via CdTe@CdS/dendrimer probe and Au nanoparticle quencher. *Biosens. Bioelectron.* **2018**, *102*, 328−335.

(13) Liao, N.; Zhong, X.; Liang, W.-B.; Yuan, R.; Zhuo, Y. Metal-organic Frameworks (MOF)-based Novel Electrochemiluminescence Biosensing Platform for Quantification of H_2O_2 Releasing from Tumor Cells. *Acta Chim. Sinica* **2021**, *79*, 1257−1264.

(14) Wang, B.; Pan, M.; Zhuo, Y. Construction of Electrochemiluminescence Sensing Interface Based on Silver Nanoclusters-Silica Nanoparticles and Biomolecular Recognition. *Chem. J. Chinese Universities* **2021**, *42*, 3519−3525.

(15) Liao, N.; Zhang, J.; Huang, Z.; Zhao, Y.; Chai, Y.; Yuan, R.; Zhuo, Y. Construction of High Efficiency Uric Acid Sensor Based on the co-Crystal Enhanced Electrochemiluminescence from 9, 10-Diphenylanthracene-perylene Microcrystals. *J. Chinese Universities* **2020**, *41*, 1989−1995.

(16) Zhuang, Y.-P.; Zhang, M.-T.; Li, X.-Y.; Zhao, M.-G.; Wang, C.-Y.; Chen, S.-G. Design of high-performance electrochemistry sensors: Elucidation of detection mechanism by DFT studies. *J. Electroanal. Chem.* **2020**, *860*, 113905.

(17) Zhao, M.; Guo, Y.-S.; Fu, G.-D.; Xue, A.-Q.; Shao, Q.-H.; Wang, Q.; Guo, D.-S. A novel near-infrared optical and redox-active receptor for the multi-model detection of Hg^{2+} in water and living cells. *Spectrochim. Acta, Part A* **2021**, *248*, 119252.

(18) Chen, M.; Mo, F.-J.; Meng, H.; Wang, C.; Guo, J.; Fu, Y.-Z. Efficient Curing Sacrificial Agent-Induced Dual-Heterojunction Photoelectrochemical System for Highly Sensitive Immunoassay. *Anal. Chem.* **2021**, *93*, 2464−2470.

(19) Song, M.-L.; Sun, H.-H.; Yu, J.; Wang, Y.; Li, M.-F.; Liu, M.-C.; Zhao, G.-H. Enzyme-Free Molecularly Imprinted and Graphene-Functionalized Photoelectrochemical Sensor Platform for Pollutants. *ACS Appl. Mater. Interfaces* **2021**, *13*, 37212−37222.

(20) Huang, L.-J.; Yang, L.; Zhu, C.-C.; Deng, H.-M.; Liu, G.-P.; Yuan, Y.-L. Methylene Blue Sensitized Photoelectrochemical Biosensor with 3,4,9,10-Perylene Tetracarboxylic Acid Film as Photoelectric Material for Highly Sensitive Pb^{2+} Detection. *Sensors Actuators B Chem.* **2018**, *274*, 458−463.

(21) Li, Y.; Chen, F.-T.; Luan, Z.-Z.; Zhang, X.-R. A versatile cathodic "signal-on" photoelectrochemical platform based on a dual-signal amplification strategy. *Biosens. Bioelectron.* **2018**, *119*, 63−69.

https://doi.org/10.1021/acsomega.2c01335
ACS Omega 2022, 7, 19622−19630

(22) Zhao, C.-R.; Zhang, L.-Y.; Wang, Q.; Zhang, L.-T.; Zhu, P.-H.; Yu, J.-H.; Zhang, Y. Porphyrin-Based Covalent Organic Framework Thin Films as Cathodic Materials for "On-Off-On" Photoelectrochemical Sensing of Lead Ions. *ACS Appl. Mater. Interfaces* **2021**, *13*, 20397−20404.
(23) Wang, Y.-Z.; Zu, M.; Zhou, X.-S.; Lin, H.; Peng, F.; Zhang, S.-Q. Designing efficient TiO_2-based photoelectrocatalysis systems for chemical engineering and sensing. *Chem. Eng. J.* **2020**, *381*, 122605.
(24) Gao, B.-W.; Zhao, X.; Liang, Z.-S.; Wu, Z.-F.; Wang, W.; Han, D.-X.; Niu, L. CdS/TiO_2 Nanocomposite-Based Photoelectrochemical Sensor for a Sensitive Determination of Nitrite in Principle of Etching Reaction. *Anal. Chem.* **2021**, *93*, 820−827.
(25) Xia, L.-Y.; Tang, Y.-N.; Zhang, J.; Dong, T.-Y.; Zhou, R.-X. Advances in the DNA Nanotechnology for the Cancer Biomarkers Analysis: Attributes and Applications. *Semin. Cancer Biol.* **2022**, DOI: 10.1016/j.semcancer.2021.12.012.
(26) Yan, X.-H.; Li, G.; Yu, Z.-C.; Liu, G.-H.; Yang, C.-P.; Hu, J.-F.; Wang, K.-Y. Advances in Magnetic-Field Assisted Photoelectrochemical Systems for Highly Efficient Conversion of Renewable Energy. *Adv. Mater. Interfaces* **2021**, *8*, 2100446.
(27) Ye, C.; Wu, Z.; Ma, K.-Y.; Xia, Z.-H.; Pan, J.; Wang, M.-Q.; Ye, C.-H. Ti_3C_2 MXene-based Schottky photocathode for enhanced photoelectrochemical sensing. *J. Alloy. Compd.* **2021**, *859*, 157787.
(28) Di, Y.-W.; Ma, C.; Fu, Y.-H.; Dong, X.-L.; Liu, X.-H.; Ma, H.-C. Engineering Cationic Sulfur-Doped Co_3O_4 Architectures with Exposing High-Reactive (112) Facets for Photoelectrocatalytic Water Purification. *ACS Appl. Mater. Interfaces* **2021**, *13*, 8405−8416.
(29) Xu, R.; Du, Y.; Ma, H.-M.; Wu, D.; Ren, X.; Sun, X.; Wei, Q.; Ju, H.-X. Photoelectrochemical aptasensor based on $La_2Ti_2O_7/Sb_2S_3$ and V_2O_5 for effectively signal change strategy for cancer marker detection. *Biosens. Bioelectron.* **2021**, *192*, 113528.
(30) Xia, L.-Y.; Li, M.-J.; Wang, H.-J.; Yuan, R.; Chai, Y.-Q. Novel Single-Enzyme-Assisted Dual Recycle Amplification Strategy for Sensitive Photoelectrochemical MicroRNA Assay. *Anal. Chem.* **2020**, *92*, 14550−14557.
(31) Deng, H.-M.; Chai, Y.-Q.; Yuan, R.; Yuan, Y.-L. In Situ Formation of Multifunctional DNA Nanospheres for a Sensitive and Accurate Dual-Mode Biosensor for Photoelectrochemical and Electrochemical Assay. *Anal. Chem.* **2020**, *92*, 8364−8370.
(32) Li, X.; Lu, J.-M.; Feng, L.-Z.; Zhang, L.-Z.; Gong, J.-M. Smart pH-Regulated Switchable Nanoprobes for Photoelectrochemical Multiplex Detection of Antibiotic Resistance Genes. *Anal. Chem.* **2020**, *92*, 11476−11483.
(33) Cao, X.-S.; Yue, L.; Lian, F.; Wang, C.-X.; Cheng, B.-X.; Lv, J.-Z.; Wang, Z.-Y.; Xing, B.-S. CuO nanoparticles doping recovered the photocatalytic antialgal activity of graphitic carbon nitride. *J. Hazard. Mater.* **2021**, *403*, 123621.
(34) Zhang, X.; Yang, P.; Jiang, S.-P. The edge-epitaxial growth of yellow g-C_3N_4 on red g-C_3N_4 nanosheets with superior photocatalytic activities. *Chem. Commun.* **2021**, *57*, 3119−3122.
(35) Qian, X.-Y.; Meng, X.-Q.; Sun, J.-W.; Jiang, L.-L.; Wang, Y.-N.; Zhang, J.-L.; Hu, X.-M.; Shalom, M.; Zhu, J.-W. Salt-Assisted Synthesis of 3D Porous g-C_3N_4 as a Bifunctional Photoand Electrocatalyst. *ACS Appl. Mater. Interfaces* **2019**, *11*, 27226−27232.
(36) Wu, J.; Tian, L.-L.; Duan, H.-M.; Cheng, Y.-H.; Shi, L. Unveiling the Working Mechanism of g-C_3N_4 as a Protection Layer for Lithium- and Sodium-Metal Anode. *ACS Appl. Mater. Interfaces* **2021**, *13*, 46821−46829.
(37) Jin, Y.-C.; Kang, Q.; Guo, X.-L.; Zhang, B.; Shen, D.-Z.; Zou, G.-Z. An Electrochemical Signal-Amplification Strategy for Electrochemiluminescent Immunoassay with g-C_3N_4 as Tags. *Anal. Chem.* **2018**, *90*, 12930−12936.
(38) Huang, D.-L.; Li, Z.-H.; Zeng, G.-M.; Zhou, C.-Y.; Xue, W.-J.; Gong, X.-M.; Yan, X.-L.; Chen, S.; Wang, W.-J.; Cheng, M. Megamerger in photocatalytic field: 2D g-C_3N_4 nanosheets serve as support of 0D nanomaterials for improving photocatalytic performance. *Appl. Catal. B Environ* **2019**, *240*, 153−73.
(39) Mao, L.-B.; Xue, X.-J.; Xu, X.; Wen, W.; Chen, M.-M.; Zhang, X.-H.; Wang, S.-F. Heterostructured CuO-g-C_3N_4 nanocomposites as a highly efficient photocathode for photoelectrochemical aflatoxin B1 sensing. *Sensors Actuators B Chem.* **2021**, *329*, 129146.
(40) Chen, X.; Zhang, W.-W.; Zhang, L.-X.; Feng, L.-P.; Zhang, C.-X.; Jiang, J.; Wang, H. Turning on the Photoelectrochemical Responses of Cd Probe-Deposited g-C_3N_4 Nanosheets by Nitrogen Plasma Treatment toward a Selective Sensor for H_2S. *ACS Appl. Mater. Interfaces* **2021**, *13*, 2052−2061.
(41) Xu, Y.-H.; Wen, Z.-R.; Wang, T.-S.; Zhang, M.; Ding, C.-F.; Guo, Y.-S.; Jiang, D.; Wang, K. Ternary Z-scheme heterojunction of Bi SPR-promoted $BiVO_4$/g-C_3N_4 with effectively boosted photoelectrochemical activity for constructing oxytetracycline aptasensor. *Biosens. Bioelectron.* **2020**, *166*, 112453.
(42) Zhang, L.-X.; Feng, L.-P.; Li, P.; Chen, X.; Xu, C.-C.; Zhang, S.; Zhang, A.-C.; Chen, G.-F.; Wang, H. Near-infrared light-driven photoelectrochemical sensor for mercury (II) detection using bead-chain-like Ag@Ag_2S nanocomposites. *Chem. Eng. J.* **2021**, *409*, 128154.
(43) Xiao, F.-X.; Liu, B. Plasmon-Dictated Photo-Electrochemical Water Splitting for Solar-to-Chemical Energy Conversion: Current Status and Future Perspectives. *Adv. Mater. Interfaces* **2018**, *5*, 1701098.
(44) Wang, D.-D.; Ding, Z.-Y.; Zhou, H.; Chen, L.-P.; Feng, X.-J. Au Nanoparticle-Decorated TiO_2 Nanowires for Surface Plasmon Resonance-Based Photoelectrochemical Bioassays with a Solid-Liquid-Air Triphase Interface. *ACS Appl. Nano Mater.* **2021**, *4*, 9401−9408.
(45) Xu, Y.; Jiang, D.; Zhang, M.; Zhang, Z.-Z.; Qian, J.; Hao, N.; Ding, C.-F.; Wang, K. High-performance photoelectrochemical aptasensor for enrofloxacin based on Bi-doped ultrathin polymeric carbon nitride nanocomposites with SPR effect and carbon vacancies. *Sensors Actuators B Chem.* **2020**, *316*, 128142.
(46) Da, H.-M.; Liu, H.-Y.; Zheng, Y.-N.; Yuan, R.; Chai, Y.-Q. A highly sensitive VEGF(165) photoelectrochemical biosensor fabricated by assembly of aptamer bridged DNA networks. *Biosens. Bioelectron.* **2018**, *101*, 213−218.
(47) Deiminiat, B.; Rounaghi, G.-H. A novel visible light photoelectrochemical aptasensor for determination of bisphenol A based on surface plasmon resonance of gold nanoparticles activated g-C_3N_4 nanosheets. *J. Electroanal. Chem.* **2021**, *886*, 115122.
(48) Wu, L.; Hu, Y.-F.; Sha, Y.-H.; Li, W.-R.; Yan, T.-T.; Wang, S.; Li, X.; Guo, Z.-Y.; Zhou, J.; Su, X.-R. An "in-electrode"-type immunosensing strategy for the detection of squamous cell carcinoma antigen based on electrochemiluminescent AuNPs/g-C_3N_4 nanocomposites. *Talanta* **2016**, *160*, 247−255.
(49) Gu, Y.; Hu, Y.-L.; Zhang, F.-Y.; Yi, L.-Z.; Shang, Y.; Ren, D.-B.; Ge, Z.-H. Electrochemiluminescence sensor based on cyclic peptides-recognition and Au nanoparticles assisted graphitic carbon nitride for glucose determination. *Microchim Acta* **2021**, *188*, 151.
(50) Gu, C.-C.; Hou, T.; Zhang, S.-X.; Gai, P.-P.; Li, F. Light-driven ultrasensitive self-powered cytosensing of circulating tumor cells via integration of biofuel cells and a photoelectrochemical strategy. *J. Mater. Chem. B* **2019**, *7*, 2277−2283.
(51) Xu, L.; Ling, S.-Y.; Li, H.-N.; Yan, P.-C.; Xia, J.-X.; Qiu, J.-X.; Wang, K.; Li, H.-M.; Yuan, S.-Q. Photoelectrochemical monitoring of 4-chlorophenol by plasmonic Au/graphitic carbon nitride composites. *Sens. Actuators B* **2017**, *240*, 308−314.
(52) Tang, L.; Ouyang, X.-L.; Peng, B.; Zeng, G.-M.; Zhu, Y.; Yu, J.-F.; Feng, C.-Y.; Fang, S.-Y.; Zhu, X.; Tan, J.-S. Highly sensitive detection of microcystin-LR under visible light using a self-powered photoelectrochemical aptasensor based on a CoO/Au/g-C_3N_4 Z-scheme heterojunction. *Nanoscale* **2019**, *11*, 12198−12209.
(53) Tao, X.-L.; Pan, M.-C.; Yang, X.; Yuan, R.; Zhuo, Y. CDs assembled metal-organic framework: Exogenous coreactant-free biosensing platform with pore confinement-enhanced electrochemiluminescence. *Chin. Chem. Lett.* **2022**, DOI: 10.1016/j.cclet.2022.01.010.
(54) Zhang, Q.-L.; Yang, S.-Y.; Yin, S.-N.; Xue, H.-G. Over two-orders of magnitude enhancement of the photocatalytic hydrogen

evolution activity of carbon nitride via mediator-free decoration with gold-organic microspheres. *Chem. Commun.* **2017**, *53*, 11814−11817.
(55) Li, M.-J.; Zheng, Y.-N.; Liang, W.-B.; Yuan, R.; Chai, Y.-Q. Using p-type PbS Quantum Dots to Quench Photocurrent of Fullerene-Au NP@MoS_2 Composite Structure for Ultrasensitive Photoelectrochemical Detection of ATP. *ACS Appl. Mater. Interfaces* **2017**, *9*, 42111−42120.
(56) Li, Z.-H.; Sun, H.-J.; Ma, X.-Y.; Su, R.-F.; Sun, R.; Yang, C.-Y.; Sun, C.-Y. Label-free fluorescence "turn-on" strategy for mercury (II) detection based on the T-Hg^{2+}-T configuration and the DNA-sensitized luminescence of terbium (III). *Anal. Chim. Acta* **2020**, *1099*, 136−144.
(57) Subedi, S.; Neupane, L.-N.; Yu, H.; Lee, K.-H. A new ratiometric fluorescent chemodosimeter for sensing of Hg^{2+} in water using irreversible reaction of arylboronic acid with Hg^{2+}. *Sens. Actuators B Chem.* **2021**, *338*, 129814.
(58) Qi, L.; Xiao, M.-S.; Wang, F.; Wang, L.-H.; Ji, W.; Man, T.-T.; Aldalbahi, A.; Khan, M. N.; Periyasami, G.; Rahaman, M.; Alrohaili, A.; Qu, X.-M.; Pei, H.; Wang, C.; Li, L. Poly-cytosine-mediated nanotags for SERS detection of Hg^{2+}. *Nanoscale* **2017**, *9*, 14184−14191.
(59) Zhang, M.; Qu, Y.; Li, D.-X.; Liu, X.-Y.; Niu, Y.-S.; Xu, Y.-H. To Love and to Kill: Accurate and Selective Colorimetry for Both Chloride and Mercury Ions Regulated by Electro-Synthesized Oxidase-like SnTe Nanobelts. *Anal. Chem.* **2021**, *93*, 10132−10140.
(60) Lan, L.-X.; Niu, Q.-F.; Li, T.-D. A highly selective colorimetric and ratiometric fluorescent probe for instantaneous sensing of Hg^{2+} in water, soil and seafood and its application on test strips. *Anal. Chim. Acta* **2018**, *1023*, 105−114.
(61) Bushira, F. A.; Kitte, S. A.; Xu, C.; Li, H.-J.; Zheng, L.-R.; Wang, P.; Jin, Y.-D. Two-Dimensional-Plasmon-Boosted Iron Single-Atom Electrochemiluminescence for the Ultrasensitive Detection of Dopamine, Hemin, and Mercury. *Anal. Chem.* **2021**, *93*, 9949−9957.
(62) Yang, X.-Y.; Zhang, M.-J.; Chen, Z.-X.; Bu, Y.-W.; Gao, X.; Sui, Y.-K.; Yu, Y.-Q. Sodium Alginate Micelle-Encapsulating Zinc Phthalocyanine Dye-Sensitized Photoelectrochemical Biosensor with CdS as the Photoelectric Material for Hg^{2+} Detection. *ACS Appl. Mater. Interfaces* **2021**, *13*, 16828−16836.

https://doi.org/10.1021/acsomega.2c01335
ACS Omega 2022, 7, 19622−19630